

ESO-Large Program on TNOs: Near-infrared spectroscopy with SINFONI[☆]

Aurélie Guilbert^{a,*}, Alvaro Alvarez-Candal^a, Frédéric Merlin^{a,b}, Maria Antonietta Barucci^a, Christophe Dumas^c, Catherine de Bergh^a, Audrey Delsanti^a

^a LESIA, Observatoire de Paris Section Meudon, 5 Place Jules Janssen, F-92195 Meudon Principal Cedex, France

^b Department of Astronomy, University of Maryland, College Park, MD 20742, USA

^c ESO, Alonso de Cordova 3107, Vitacura, casilla 19001, Santiago 19, Chile

ARTICLE INFO

Article history:

Received 16 May 2008

Revised 12 December 2008

Accepted 15 December 2008

Available online 31 December 2008

Keywords:

Centaur

Kuiper belt

Infrared observations

ices

ABSTRACT

We present in this work the observations performed with SINFONI in the framework of a new ESO-Large Program (2006–2008) on Trans-Neptunian Objects (TNOs) and Centaurs. We obtained 21 near-infrared (1.49 to 2.4 microns) spectra of high quality, including 4 spectra of objects never observed before. We search for the presence of features due to ices, particularly water ice. Eris is the only object showing deep methane ice absorption bands. The spectra of 4 objects are featureless, and 6 others show clearly the presence of water ice. For 7 objects, the detections are more ambiguous, but absorption bands could be embedded in the noise. The 3 remaining spectra are too noisy to draw any reliable conclusion. The possible amount of water ice on each object's surface has been computed. The analysis shows that some objects present strong compositional heterogeneities over the surface (e.g. Chariklo), while some others are completely homogeneous (e.g. Quaoar).

© 2009 Elsevier Inc. All rights reserved.

1. Introduction

More than a thousand Trans-Neptunian Objects (TNOs) have been detected since the first discovery, in 1992 (Jewitt and Luu, 1993). Considered as pristine remnants of planet formation, they are believed to provide clues to constrain the early stages of Solar System evolution. Nonetheless, because of their great distance from the Sun, and their resulting faintness, their physical properties are still hard to access. Much effort has been made in the past decade to improve our understanding of TNOs and their related populations such as Centaurs. Broadband photometric observations have been performed for more than a hundred objects (Doressoundiram et al., 2008), but spectroscopic information is far more difficult to obtain, and only a small number of spectra are available. TNOs and Centaurs display a wide range of colors, from slightly blue-neutral to very red. Visible spectra are mostly featureless, showing a great variety of spectral slopes that confirm the corresponding colors. The overtones and combination bands of chemical bonds such as O–H, N–H or C–H can be seen in the near-infrared wavelength range. Near-infrared spectra are thus very helpful to search for the presence of ices. The available near-infrared spectra are very diverse. The spectral behaviors change from featureless to showing absorption bands due to the presence of water, methane, methanol

or nitrogen ices for example (see Barucci et al., 2008b and references therein for a review).

The observed colors and spectra are thought to be the result of the competition between several processes leading to different alteration states of TNOs' surfaces. Some of the reddest objects tend to show a featureless spectrum, which is consistent with the idea that TNOs' surfaces are made of an irradiated crust, obscuring the absorption bands due to the presence of ices underneath. Indeed, laboratory studies show that irradiated ices become redder with an increasing irradiation dose. Irradiation results in a progressive polymerization of the surface layer (Strazulla and Palumbo, 1998), and the formation of a crust that can reach a meter-thick within 10^{7-9} years (Shul'man, 1972). Brunetto and Roush (2008) have recently shown that a crust made of irradiated methane of 10 μm is sufficient to hide the water ice underneath in the spectra. Some effect is also expected on the albedo. Indeed, Thompson et al. (1987) showed that irradiation of fresh blue ice with high albedo induces a drop of the albedo at shorter wavelengths, resulting in the reddening of the surface. When increasing the irradiation dose, the albedo finally drops at all wavelengths to reach a very low value, associated with a neutral color. On the other hand, collisions tend to expose underlying non-irradiated material, resulting in a refreshment of the surface. Cometary activity acts in the same way, by redepositing fresh, sublimated material on the surface. Such activity has been observed at large distances from the Sun (Meech and Belton, 1990; Rousselot, 2008) and even suspected for TNOs (Hainaut et al., 2000). The presence of crystalline water ice, or ammonia hydrates on the surface of some objects suggests a recent

[☆] Observations performed in the framework of ESO-Large Program 178.C-0036.

* Corresponding author.

E-mail address: aurelie.guilbert@obspm.fr (A. Guilbert).

surface renewal, since these materials should be depleted of surfaces in less than 10^7 years by irradiation (Cooper et al., 2003). This raises the question of possible internal activity that can bring to the surface unirradiated material (Cook et al., 2007). Studies on the internal activity of TNOs have shown that some of them can remain very primitive, while some others can be highly processed and even differentiated (De Sanctis et al., 2001; McKinnon, 2002; Merk and Prrialnik, 2006).

Therefore, our current knowledge of TNOs leads to a very complicated picture, requiring further studies. A new ESO-Large Program has been undertaken since October 2006 with the aim of collecting comprehensive visible and near-infrared spectral and photometric information on about 40 objects. Three main instruments are used, for a total amount of about 500 h, to perform simultaneous observations at high S/N needed to unambiguously detect and quantify compounds present at the surface of each object: FORS1/2 (V, R and I bands photometry, visible spectroscopy), ISAAC (J, H and K bands photometry and J spectroscopy) and SINFONI (simultaneous H + K spectroscopy). Additional observations – light curves (Dotto et al., 2008) and polarimetry (Belskaya et al., 2008) – are also carried out to build as complete a portrait as possible of a few selected objects. First results concerning visible and near-infrared photometry will be presented in DeMeo et al. (2009), while visible spectroscopy is presented in Alvarez-Candil et al. (2008). This paper presents the observations performed with SINFONI during the first year of this Large Program, along with data reduction, in Section 2. The 21 spectra and other related results will be shown in Section 3, and discussed in Section 4.

2. Observations and data reduction

2.1. Observations

SINFONI is a near-infrared integral field spectrometer, installed on UT4-“Yepun” ESO-VLT. It is built from two components: the

Spectrograph for Integral Faint Field Imaging (SPIFFI) developed by MPE (Max-Planck-Institut für Extraterrestrische Physik) and NOVA (Nederlands Onderzoekschool Voor Astronomie) (Eisenhauer et al., 2003), and the Multi-Application Curvature Adaptive Optics unit (MACAO) developed by ESO. The instrument is equipped with a Rockwell Hawaii 2RD detector of 2048×2048 pixels, and observations can be done either using the AO mode in Natural Guide Star mode, or in Laser Guide Star mode, or in seeing limited conditions. Each image taken with SINFONI is optically cut into 32 strips, that are then spectrally dispersed and re-imaged onto 64 pixels of the detector. We chose to use the H + K grating which provides a spectral resolution of about 1500 over the 1.45–2.45 μm wavelength range, and the widest field of view ($8'' \times 8''$) which provides a spatial resolution element of 125×250 mas. The observations were carried out in seeing limited mode.

Science observations were performed using the auto-jitter template, that shifts the telescope between two elementary exposures according to a random pattern. Offsets are distributed within a box, whose size is user defined. This size is determined as a balance between a good overlap between different frames (given by a small box), and a good estimation of the sky (given by a large box). The observations of a given object were centered in time – when possible – on its meridian transit to ensure a stable airmass. A solar analog was observed with the same instrumental settings and with an airmass as close as possible to the target airmass, so to provide the needed calibrations. Twenty-one Centaurs and trans-neptunian objects (see Table 1) have been observed using this technique during ESO-periods 78 and 79 (from October 2006 to September 2007), both in visitor and service mode. Good observational conditions (Table 1) – stable sky and seeing, low airmasses – ensure a good sky estimation and correction on each elementary frame, and a good removal of solar response and telluric features from the objects' spectra.

Table 1
Observational circumstances.

Number	Name	Class	Date ^a	Exp. ^b	Airmass ^c	Seeing ^d	Analog ^e	Airm. ^f
10199	Chariklo	Cen	Mar 20, 07	80	1.017–1.041	1.0''	SA 107–998	1.212
15874	1996 TL ₆₆	TNO	Jan 24, 07	160	1.258–1.510	1.4''*	Ld 98–978	1.178
26375	1999 DE ₉	TNO	Jan 22, 07	150	1.110–1.295	0.6''	Ld 98–978	1.176
28978	Ixion	TNO	Jul 15, 07	70	1.168–1.484	1.5''*	HD 147–935	1.163
32532	Thereus	Cen	Sep 19, 07	150	1.221–1.389	1.4''*	Hyades 64	1.346
42355	Typhon	TNO	Jan 24, 07	150	1.209–1.347	0.6''	Ld 102–1081	1.189
47171	1999 TC ₃₆	TNO	Nov 08, 07	100	1.078–1.120	0.7''	HD 2966	1.059
47932	2000 GN ₁₇₁	TNO	Mar 24, 07	100	1.065–1.370	1.0''*	SA 107–998	1.204
50000	Quaoar	TNO	Jul 15, 07	100	1.014–1.080	1.2''	Hd 147–935	1.163
54598	Bienor	Cen	Sep 18, 07	150	1.118–1.323	1.5''*	Ld 112–1333	1.170
55565	2002 AW ₁₉₇	TNO	Jan 23, 07	130	1.169–1.365	0.8''	Ld 98–978	1.207
60558	Echeclus	Com	May 15, 07	100	1.052–1.098	0.5''	SA 107–684	1.129
83982	Crantor	Cen	Jul 14, 07	100	1.032–1.197	0.8''	SA 110–361	1.104
90482	Orcus	TNO	Jan 25, 07	100	1.080–1.099	0.8''	Ld 98–978	1.102
90568	2004 GV ₉	TNO	May 13, 07	150	1.002–1.368	0.6''	HD 147–935	1.112
119951	2002 KX ₁₄	TNO	Jul 14, 07	110	1.002–1.124	0.8''	HD 147–935	1.002
120132	2003 FY ₁₂₈	TNO	Jan 23, 07	40	1.039–1.066	1.0''*	Ld 102–1081	1.106
136199	Eris	TNO	Oct 20, 06	100	1.060–1.157	0.7''	Ld 93–101	1.106
145452	2005 RN ₄₃	TNO	Sep 19, 06	210	1.097–1.379	1.5''*	HD 1368	1.156
	2003 AZ ₈₄	TNO	Jan 25, 07	100	1.262–1.352	1.2''*	Ld 102–1081	1.379
	2003 QW ₉₀	TNO	Nov 10, 06	100	1.086–1.142	0.7''	HD 1368	1.115

^a Observation date.

^b Exposure time in minutes for the spectra in the H + K band.

^c Airmass range achieved during the whole exposure time.

^d Visible seeing given by the astronomical seeing monitor during the whole exposure time. The value is stable except when marked by *, which means that the sky was not stable during the observations, leading sometimes to large variations of the seeing. In this case, an average value is given.

^e Solar analog used to correct for solar response and telluric features.

^f Solar analog airmass, taken as close as possible from the value of the science target airmass.

2.2. Data reduction

The first step of the data reduction is a cleaning of all science and calibration frames of bad lines. These are created by the data processing, in particular the estimation of the bias level, hard-coded at the detector level, and are not stable since they depend on the exposure time. The following data reduction steps have been performed using SINFONI pipeline version 1.7, developed by ESO. Flat fields taken with increasing intensity are first used to compute the detector's linearity, and create a map of highly non-linear bad pixels. A master dark and a map of hot pixels are created from the median of a series of dark frames. Finally, flat field frames with constant intensity are required to compute the master flat field and a third bad pixels map. Those three bad pixels maps are then combined to generate a master bad pixels map. Geometric distortions are determined using frames obtained by placing a fiber at different positions on the detector. Each science or solar analog frame is therefore corrected for the dark, bad pixels, distortions and flat fielded. The wavelength calibration is provided by Xenon arc lamp frames.

We paid a special attention to the sky estimation and subtraction, which is critical when dealing with our faint objects. Since the objects are not extended, the SINFONI field of view is wide enough to provide a good sky estimation. Nonetheless, some tests were made with independent sky images, but they did not produce any noticeable improvement on the sky correction. The pipeline provides two methods to estimate and correct for the sky. The first one, which computes the median of all images as an estimation of the sky, is not accurate especially when the sky is not stable. The second method, which we chose for our data reduction, uses the closest frame in time as an estimation of the sky to be subtracted. In any case, a sky residual correction based upon a method developed by Davies (2007) can be applied. This improves slightly the S/N for brighter objects, but no dramatic change has been noticed in the spectra of the fainter ones.

All frames are then shifted and co-added. They contain both spectral and spatial information, and are therefore reconstructed to

produce 3D cubes. The 1D spectra are extracted using QFitsView, a 3D visualization tool developed by MPE. The size of the extraction aperture — the same for the science target and the corresponding solar analog — is determined as a compromise between the maximum gathered flux and the minimum sky residual contribution, and was found to have no influence on the spectral gradient. The target spectrum is finally divided by the solar analog spectrum and cleaned of spikes and bad pixel residuals. Since the spectral resolution is high (about 1500 in the H band), it is possible to rebin the data in order to increase the signal to noise ratio, but at the price of a lower resolution. We therefore applied a smoothing (the same for all objects to allow direct comparison) resulting in a spectral resolution of about 100. Each spectrum has finally been normalized to 1 around 1.65 microns, in the 1.5–1.8 microns region corresponding to the photometric broadband filter used for ISAAC observations.

3. Results

The 21 spectra are shown in Figs. 1, 2 and 3. The dotted lines correspond to the cleaned spectra, and solid lines to smoothed spectra. Fig. 1a shows the spectra of Orcus, Quaoar, 2003 AZ₈₄, Bienor and Typhon, and Fig. 1b shows the spectra of Thereus, Chariklo, 2004 GV₉, 2002 KX₁₄, 2005 RN₄₃. Fig. 2a shows the spectra of Ixion, 1999 TC₃₆, Crantor, Echeclus and 2002 AW₁₉₇ while Fig. 2b shows the spectra of 1999 DE₉, 2000 GN₁₇₁, 2003 FY₁₂₈, 2003 QW₉₀ and 1996 TL₆₆. Eris's spectrum is presented in Fig. 3. Physical characteristics such as albedo or radius of each object can be found in Table 2.

The 21 spectra show very different behaviors. Eris's spectrum shows deep absorption bands attributed to the presence of methane ice on its surface (Fig. 3). Absorption bands due to water ice (1.5 and 2.2 microns) are detected on Orcus and Quaoar (Fig. 1a). Those two spectra also show the 1.65 microns absorption band due to the presence of water ice in its crystalline phase, as well as some feature centered at 2.2 microns, that can be attributed either to ammonia hydrates, or to methane ice. Quaoar's

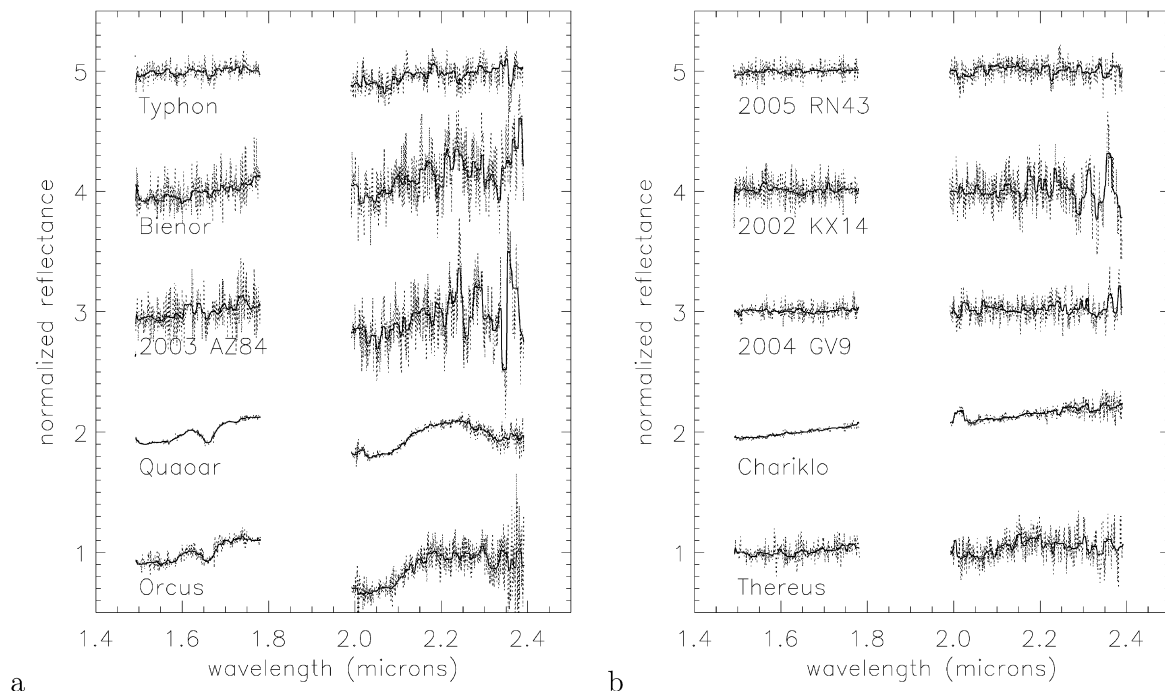


Fig. 1. Spectra of 10 objects. Dotted line corresponds to the "raw" spectrum, i.e. the object's extracted spectra divided by the solar analog spectrum (spectral resolution of 1500). The solid line corresponds to the smoothed spectrum (spectral resolution of about 100). Each spectrum has been normalized to 1 around 1.65 microns (in the 1.5–1.8 microns wavelength range corresponding to the broadband photometric filter), and then shifted in reflectance on the plot for clarity.

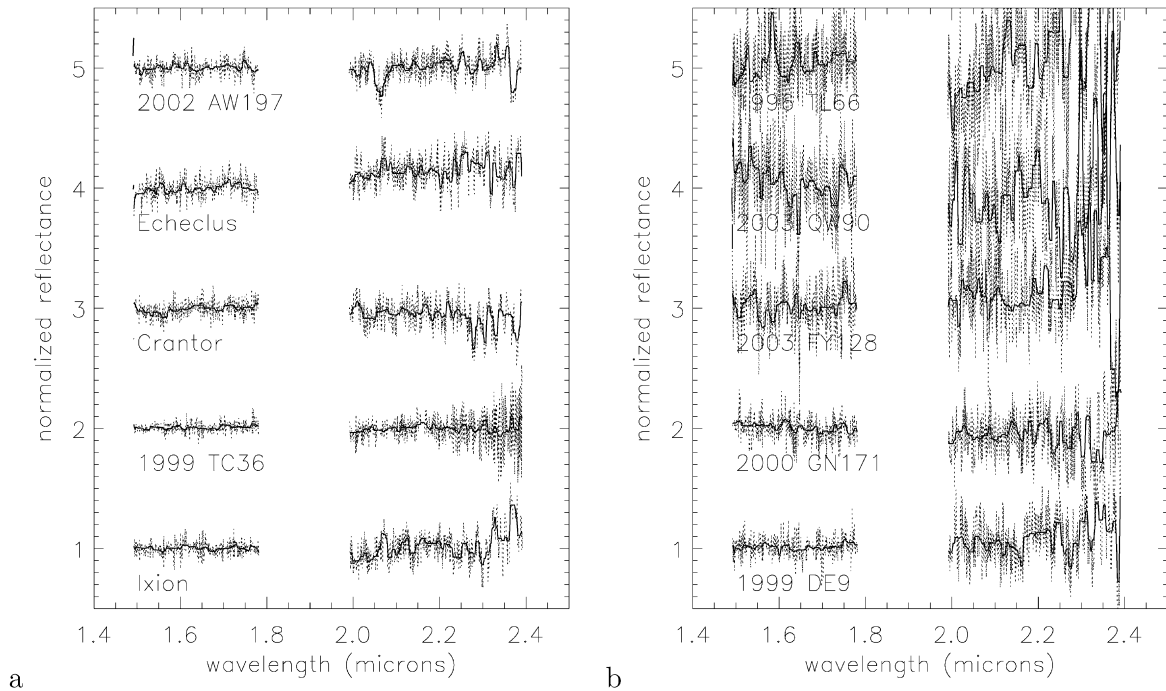


Fig. 2. Spectra of 10 objects. Dotted line corresponds to the “raw” spectrum, i.e. the object’s extracted spectra divided by the solar analog spectrum (spectral resolution of 1500). The solid line corresponds to the smoothed spectrum (spectral resolution of about 100). Each spectrum has been normalized to 1 around 1.65 microns (in the 1.5–1.8 microns wavelength range corresponding to the broadband photometric filter), and then shifted in reflectance on the plot for clarity.

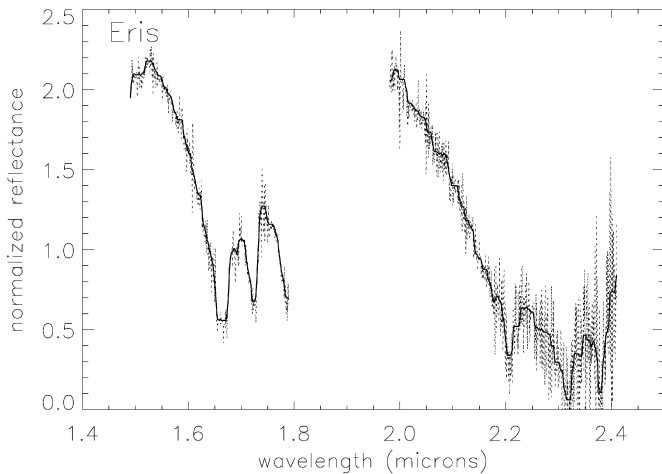


Fig. 3. Spectrum of Eris. The dotted line corresponds to the “raw” spectrum, i.e. the object’s extracted spectra divided by the solar analog spectrum (spectral resolution of 1500). The solid line corresponds to the smoothed spectrum (spectral resolution of about 100). The spectrum has been normalized to 1 around 1.65 microns (in the spectral region corresponding to the broadband photometric filter).

spectrum also shows a small feature centered at 1.724 microns that we attribute to methane ice. For a few other objects (2003 AZ₈₄, Bienor, Typhon and Thereus) the 2.0 microns absorption band due to water ice can be detected (Fig. 1). Nonetheless, no corresponding feature can be detected at 1.5 micron. In the case of Crantor, 1999 TC₃₆, Ixion, Echeclus, 1999 DE₉, 2000 GN₁₇₁ and 2002 AW₁₉₇, no feature is visible in their spectra, but the level of noise could hide some bands due to ices. Four other spectra are featureless within the noise level: 2004 GV₉, 2002 KX₁₄, 2005 RN₄₃ and Chariklo. 1996 TL₆₆, 2003 QW₉₀ and 2003 FY₁₂₈ show very noisy spectra that do not allow a meaningful search for absorption bands.

The main goal of our analysis is to constrain the water ice amount that can be present on the objects’ surface, and to com-

pare them with one another. We therefore used several tools to determine first if water ice could be present, and then to quantify its amount. For this purpose, we computed the spectral gradient in the H + K region, and paid a particular attention to the spectral shape (featureless or not). Then we tried to determine whether the 2.0 microns absorption band characteristic of water ice was present or not, and computed its depth. At last, we used a simple spectral modeling to determine the water ice quantity.

The spectral gradient in the H + K region is computed by performing a linear regression over the 1.49–2.3 microns wavelength range. The region of telluric bands (from 1.8 to 1.95 microns) is excluded from the calculation to avoid any influence of this noisy part of spectra. We also exclude the region beyond 2.3 microns, where the instrument sensitivity and the resulting S/N are very low. The results are given in Table 3.

To calculate the depth of the 2.0 microns absorption band, attributed to the presence of water ice, we applied an algorithm that computes first a median of the reflectance in a 11 pixels box, centered around 1.8, 2.0 and 2.2 microns. Then a linear continuum between the median reflectance around 1.8 and 2.2 microns is determined. The depth of the band is therefore calculated relative to the continuum reflectance around 2.0 microns. Errors are computed relative to the noise level of each spectrum. The H₂O band depth is given in Table 3: it is not given for Eris, which is obviously meaningless.

At last, we applied a simple model for each spectrum – except Eris’s spectrum – using the radiative transfer method developed by Shkuratov et al. (1999). The aim is to focus on the water ice amount, and compare the objects with one another. These amounts are given in Table 3, and discussed in the next sections. We tried to limit the number of free parameters in the model; we therefore chose a simple intimate mixture, that could be applied systematically to all spectra.

Water ice should be the main component of TNOs and Centaurs, and the 1.65 microns absorption band due to crystalline water ice can be seen in some of our spectra: this implies at least a partial crystallinity of the ice. Back amorphization is ex-

Table 2
Physical properties.

Number	Name	\varnothing^a (km)	p_v^b (%)	V–H ^c	Ices prev. ^d detected	Ref.
10199	Chariklo	258 ± 11	5.8 ± 0.6	2.14 ± 0.03	H ₂ O	4, 10, 2
15874	1996 TL ₆₆	575 ± 116	3.5 ± 2.0	1.81 ± 0.17	None	18
26375	1999 DE ₉	461 ± 46	6.8 ± 1.6	2.17 ± 0.05	H ₂ O None	13 2
28978	Ixion	650 ± 260	15.6 ^{+12.0} _{-5.5}	2.18 ± 0.11	0.49 H ₂ O	15, 3, 2
32532	Thereus	88 ± 10	8.9 ± 5.3	2.1 ± 0.07	H ₂ O H ₂ O Var.	0 19, 16
42355	Typhon	175 ± 20	–	–	–	–
47171	1999 TC ₃₆	415 ± 39	7.2 ± 1.5	2.70 ± 0.03	H ₂ O	9, 19, 2
47932	2000 GN ₁₇₁	321 ± 57	5.7 ± 2.5	2.21 ± 0.14	None	6, 2
50000	Quaoar	844 ± 200	19.9 ^{+13.2} _{-7.0}	2.54 ± 0.06 ^b	H ₂ O, NH ₃ H ₂ O, CH ₄	14 20
54598	Bienor	207 ± 30	3.4 ± 1.3	2.14 ± 0.05	H ₂ O	9, 2
55565	2002 AW ₁₉₇	735 ± 116	11.8 ± 4.4	2.15 ± 0.08	H ₂ O None	8 2
60558	Echeclus	84 ± 15	3.8 ± 1.9	2.05 ± 0.12	–	–
83982	Crantor	60 ± 15	>8.6 ^{+8.6} _{-3.4}	2.83 ± 0.02	H ₂ O	8, 2
90482	Orcus	946 ± 74	19.7 ± 3.4	1.21 ± 0.04	H ₂ O H ₂ O, NH ₃ /CH ₄	12, 7, 21 1
90568	2004 GV ₉	677 ± 71	8.0 ± 1.9	1.91 ± 0.09 ^b	0.19 ± 0.31	–
119951	2002 KX ₁₄	<562 ± 220	8.1 ^{+9.6} _{-3.9}	–	None	2
120132	2003 FY ₁₂₈	–	–	–	None	2
136199	Eris	2600 ± 400	–	0.72 ± 0.04	CH ₄ CH ₄ , N ₂	5 11, 17
145452	2005 RN ₄₃	–	–	–	None	2
	2003 AZ ₈₄	686 ± 99	12.3 ± 4.3	1.28 ± 0.14	H ₂ O	2
	2003 QW ₉₀	–	–	–	–	–

^a Diameter of the object, from Stansberry et al. (2008).

^b Visual albedo from Stansberry et al. (2008).

^c V–H color from Fulchignoni et al. (2008). When noted ^b, from DeMeo et al. (2009).

^d Ices previously detected in other works. References: (0) Barucci et al. (2002), (1) Barucci et al. (2008a), (2) Barkume et al. (2008), (3) Boehnhardt et al. (2004), (4) Brown and Koresko (1998), (5) Brown et al. (2005), (6) de Bergh et al. (2004), (7) de Bergh et al. (2005), (8) Doressoundiram et al. (2005), (9) Dotto et al. (2003a), (10) Dotto et al. (2003b), (11) Dumas et al. (2007), (12) Fornasier et al. (2004), (13) Jewitt and Luu (2001), (14) Jewitt and Luu (2004), (15) Licandro et al. (2002), (16) Licandro and Pinilla-Alonso (2005), (17) Licandro et al. (2006), (18) Luu and Jewitt (1998), (19) Merlin et al. (2005), (20) Schaller and Brown (2007), (21) Trujillo et al. (2005).

pected to occur (Cooper et al., 2003), but the experience described in Zheng et al. (2008) shows that even when crystalline water ice is irradiated and amorphized, the 1.65 microns band's depth stabilizes, and the feature remains. Due to the balance between thermal recrystallization and amorphization caused by irradiation, the presence of the crystalline water ice feature can persist indefinitely (at a temperature of 40 K). Therefore, we considered crystalline water ice as the main component of our mixture. Nonetheless, previous works on water ice dominated bodies showed that a certain amount of amorphous ice was to be considered in the composition to reproduce the spectra (Merlin et al., 2007; Pinilla-Alonso et al., 2007), so that we also added amorphous water ice in our mixture. We used the optical constants from Grundy and Schmitt (1998) for crystalline water ice at 40 K, and from Schmitt et al. (1998) for amorphous ice at 38 K. We added amorphous carbon, which is a featureless dark component usually introduced to reproduce the low albedo of TNOs and Centaurs. Then, we added some compounds that could reproduce the spectral gradients: we chose ice tholins (McDonald et al., 1996) and titan tholins (Khare et al., 1993 and references therein) to reproduce the red slopes. We also decided to add a synthetic dark, blue component described in Trujillo et al. (2007) and Barucci et al. (2008a) to reproduce bluer slopes. Visual albedos (Stansberry et al., 2008) and V–H colors (Fulchignoni et al., 2008) have been used to estimate the objects' H albedo (p_H). When this estimation was not possible (lack of albedo or color), we chose an approximated albedo ($p_H = 0.1$) corresponding to a pessimistic case, leading to a lower limit to the water ice amount. The error induced in the model by

such an approximation is very small compared to errors due to optical constants or by the theory itself. It implies small changes in the relative amount of dark and light materials, which is not linear when using intimate mixtures.

A mean square algorithm is applied in order to obtain the model that best reproduces the spectrum (Merlin et al., 2007): the best fit corresponds to the composition and grains sizes that minimize the value of the reduced χ^2 . To investigate the influence of the noise, we produced synthetic models with different water ice amounts for each spectrum. The mean square algorithm has also been applied to those synthetic models to compare them with the best fit: the comparison is made by a study of the different reduced χ^2 obtained for each spectrum. In most of the cases, this comparison shows that higher amounts of water ice could be present on the spectra but embedded in the noise. Nonetheless, this assumption is true only when small changes in the ice abundance occur, otherwise the synthetic models imply too drastic changes in the albedo. These results will be briefly discussed for each object in the next section.

4. Discussion

Eris's spectrum is dominated by the presence of methane ice (see Section 4.1). The analysis of the 20 other spectra reveals three categories: featureless spectra (featureless spectral shape, no 2.0 μm band, no water ice in the model) (Section 4.2), spectra with water ice (confirmed by the shape, the depth of the 2.0 microns band and the amount found by the best fit model) (Section 4.3.1),

Table 3
Results.

Name	Gradient ^a (%/0.1 μm)	Depth ^b (%)	Am. ^c (%)	Cr. ^d (%)	Tot. ^e (%)	Gr. ^f (μm)
Crantor	-0.79 ± 0.35	6 ± 4	0	0	0	10
Echeclus	2.53 ± 0.33	*	0	0	0	10
Thereus	0.78 ± 0.33	10 ± 3	0	18	18	10
Typhon	-0.68 ± 0.35	11 ± 3	0	5	5	39
Bienor	3.23 ± 0.37	16 ± 6	0	13	13	39
Chariklo	2.89 ± 0.31	*	0	0	0	10
2000 GN ₁₇₁	-1.46 ± 0.34	4 ± 6	5	4	9	22
1999 TC ₃₆	-0.09 ± 0.32	4 ± 3	9	0	9	10
1999 DE ₉	0.85 ± 0.34	*	3	1	4	10
2002 KX ₁₄	-0.44 ± 0.33	3 ± 4	0	2	2	10
1996 TL ₆₆	0.97 ± 0.43	24 ± 11	28	0	28	23
Ixion	0.49 ± 0.33	7 ± 4	16	0	16	10
2004 GV ₉	0.19 ± 0.31	0 ± 3	1	0	1	10
2003 AZ ₈₄	-0.44 ± 0.40	17 ± 6	2	15	17	49
2002 AW ₁₉₇	0.11 ± 0.34	3 ± 7	0	17	17	10
Quaoar	0.53 ± 0.40	25 ± 2	34	42	76	10
Orcus	-2.11 ± 0.47	30 ± 3	17	15	32 ^g	20/50
2003 FY ₁₂₈	2.35 ± 0.36	*	0	1	1	10
2005 RN ₄₃	0.27 ± 0.32	1 ± 3	0	1	1	10
2003 QW ₉₀	-3.41 ± 0.49	21 ± 11	0	0	0	10

^a Near-infrared gradient of the spectrum, calculated by linear regression over the 1.43–2.3 microns range. Positive values mean that the object is brighter in K band than the H band: the object's surface is spectrally red. Negative values correspond to spectrally blue surfaces.

^b Depth of the 2.0 microns absorption band due to water ice, marked * when it is negative, which is unphysical.

^c Amount of amorphous water ice determined by the best fit model, described in Section 3.

^d Amount of crystalline water ice determined by the best fit model.

^e Total amount of water ice obtained by the best fit model.

^f Grains size of both amorphous and crystalline water ice.

^g Since Orcus has been studied in a previous article, we just mention the water ice amount (amorphous, crystalline and total), without doing any further analysis.

and ambiguous cases (see Section 4.3.2). Three spectra are too noisy to draw any reliable conclusion (Section 4.4). Each case will be discussed individually in the following sections, the results of the analysis can be found in Table 3.

4.1. The case of Eris

Eris's spectrum shows deep methane ice absorption bands (Fig. 3): we find that the surface is covered by large amounts of methane ice, which is in agreement with previous studies (Brown et al., 2005; Licandro et al., 2006; Dumas et al., 2007). And the spectral resolution achieved with the instrument allows us to measure precisely the wavelength of each absorption band. We do not find any wavelength shift in this new near-infrared spectrum, while some had been found in the visible range in previous work (Licandro et al., 2006). Such a wavelength shift suggests that part of the methane might be diluted in nitrogen. Since the layer depths probed by the visible and near-infrared spectra are not exactly the same, this suggests that Eris surface layer could be stratified (Licandro et al., 2006). A detailed analysis of this spectrum, discussed along with J and visible spectra taken simultaneously is presented in Merlin et al. (2009).

4.2. Featureless spectra

Chariklo Brown et al. (1998), Brown and Koresko (1998) and Dotto et al. (2003b) suggested the presence of water ice on Chariklo's surface, due to the presence of features at 1.5 and 2.0 microns. Though they used different spectral modeling, they all needed to add a certain amount – even small – of water ice to correctly fit their spectra. Dotto et al. (2003b) showed that possible variations

occurred, since their two spectra show different absorption bands depths. The spectrum that we present in this work shows a different behavior. It is featureless, with a very high signal to noise level (Fig. 1b), and no water ice is found (Fig. 5). This confirms that Chariklo's surface presents very compositional inhomogeneities. A special attention will be paid to Chariklo's spectral behavior and to the possible reasons for these heterogeneities in Guilbert et al. (2009), where new data will be presented.

2004 GV₉ To our knowledge, no spectrum of 2004 GV₉ had been previously published. The spectrum we present here is flat and featureless, with a spectral gradient of $0.19 \pm 0.31\%$ per 0.1 micron (Fig. 1b) and a 2.0 microns band depth of $0 \pm 3\%$. The best fit model includes 1% of amorphous water ice with 10 μm grains (Fig. 5). We therefore conclude that no significant amount of water ice is present on the surface of 2004 GV₉, within the noise.

2002 KX₁₄ No ice has been previously detected on 2002 KX₁₄ (Barkume et al., 2008). This is confirmed by our spectrum which is flat and featureless (Fig. 1b) (spectral gradient of $-0.44 \pm 0.33\%$ per 0.1 micron, and a 2.0 microns band depth of $3 \pm 4\%$). The best fit model includes 2% of crystalline water ice (10 microns grains) (Fig. 5). These results lead to the conclusion that no significant amount of water ice is present on the surface of 2002 KX₁₄.

2005 RN₄₃ Barkume et al. (2008) found that no ice was present on the surface of 2005 RN₄₃. We confirm this featureless behavior with our spectrum (Fig. 1b) (spectral gradient of $0.27 \pm 0.32\%$ per 0.1 micron, 2.0 microns band depth of $1 \pm 3\%$). The best fit model includes 1% of crystalline water ice with 10 microns grains, so that we conclude that only a negligible amount of water ice can be present in this spectrum (Fig. 5).

4.3. Water ice features

4.3.1. Unambiguous cases

Orcus We detect deep water ice absorption bands in the spectrum due to the presence of both 1.5 and 2.0 micron features. Crystalline water ice is detected by dint of the 1.65 micron absorption band, which is $12 \pm 3\%$ deep (Fig. 1a). Another feature not attributed to water ice is detected at 2.2 microns, with a depth of $10 \pm 3\%$: this can be attributed to ammonia (pure or hydrated) or methane. The Orcus's spectrum that we present here has been extensively discussed in Barucci et al. (2008a): they found a best fit model with 15% of crystalline water ice and 17% of amorphous water ice. Only small amounts of ammonia hydrates should be present on Orcus's surface. They cannot exclude the presence of small amounts of methane ice on the surface though.

Quaoar Quaoar has been first observed by Jewitt and Luu (2004). Their spectrum shows an absorption band at 1.65 microns, indicating the presence of water ice in its crystalline phase, in addition to the strong 1.5 and 2.0 micron bands. They also detect an absorption band around 2.2 microns, that they attribute to the presence of ammonia hydrates (Fig. 5). The presence on Quaoar's surface of both compounds suggested a recent resurfacing phenomenon such as cryovolcanism or comet-like activity, or alternatively impact exposure of underlying material. Recently, Schaller and Brown (2007) re-observed Quaoar with a higher signal to noise ratio in the K band, leading to a clear detection of both 1.65 and 2.2 micron features (Fig. 5). They consider the 2.2 micron feature as due to the presence of methane ice, and also include in their modelization some by-products of methane irradiation – ethane for instance – to improve the quality of the spectrum fit. We present in this work a spectrum that achieves a much higher signal to noise ratio in the H band (Fig. 4). The depth of the 2.0 micron band due to water ice

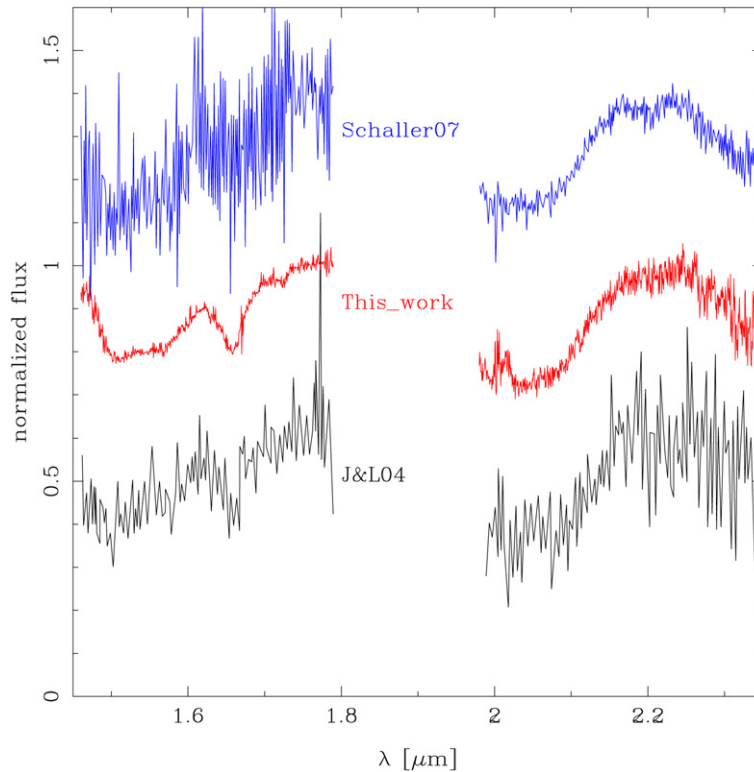


Fig. 4. *Quaoar*. H + K reflectance spectrum of *Quaoar*: Schaller and Brown (2007) (top of the plot), this work (middle of the plot, spectral resolution of 1500), Jewitt and Luu (2004) (bottom of the plot). Our spectrum achieves a much higher signal to noise ratio in the H band, leading to the unambiguous detection of the 1.65 microns band due to water ice in its crystalline phase, and of a small feature (2% deep) at 1.724 microns, attributed to methane ice. The small emission feature present in the K band is attributed to bad removal of telluric features. The K band shows the 2.0 microns water ice absorption band – which has the same depth for the three studies – and a small feature around 2.2 microns (2% deep), attributed to methane ice.

is the same for the three spectra shown in Fig. 4 (depth of about 25% within the error), which leads to the conclusion that *Quaoar*'s surface may be homogeneous. The K band also shows the 2.2 micron feature ($3 \pm 2\%$ deep) that we are inclined to attribute to methane ice, since its presence is confirmed by the 1.724 micron feature. Indeed, the high signal to noise level in the H band allows us to detect the 1.5 micron band due to water ice, the 1.65 micron band due to crystalline water ice ($14 \pm 2\%$ deep), and a 1.724 micron ($2 \pm 2\%$ deep) feature due to methane ice. We do not have evidence for the presence of a feature at 1.8 μm though. The modeling of this spectrum of unique quality, combined with visible and J spectra, is in progress in our group, and will be presented in a following article.

2003 AZ₈₄ Barkume et al. (2008) found an amount of 42% of crystalline water ice on 2003 AZ₈₄'s surface. The spectrum we observed during the Large Program is a bit noisy, but absorption bands located at 1.5, 1.65 ($11 \pm 10\%$ deep) and 2.0 microns ($17 \pm 6\%$ deep) can be detected (Fig. 1a). The best fit model is obtained with 17% of water ice (49 microns grains, see Table 3). As described in Section 3, we tried to model 2003 AZ₈₄'s spectrum with other amounts of water ice, and found that high fractions of water ice could be present (30% for example as shown on Fig. 6). We might also detect a small feature around 2.3 microns, that would be attributed to the presence of methanol. Nonetheless, the noise level in this part of the spectrum makes hard to draw reliable conclusion on this possible detection.

Bienor The spectrum observed by Dotto et al. (2003a) is rather noisy. They modeled it and added only a small amount of water ice in their model to improve the fit in the 1.5 and 2.0 microns regions. On the other hand, Barkume et al. (2008) found a larger

amount of crystalline water ice. Our spectrum shows an absorption band at 2.0 microns attributed to water ice that is $16 \pm 6\%$ deep, but no feature can be detected in the H band (Fig. 1a). We proceeded to a modeling of this spectrum in order to give a constraint on the amount of water ice that can be present on *Bienor*'s surface. The best fit model is given by a fraction of 13% of water ice with 39 microns grains (Fig. 7). We tried to model *Bienor*'s reflectance spectrum with other amounts of water ice. We show in Fig. 7 three models that can correctly fit the spectrum within the noise. A small feature around 2.3 microns due to methanol could also be present on this spectrum, but as for 2003 AZ₈₄, the noise level in this part of the spectrum does not allow us to draw reliable conclusions on this detection.

Typhon To our knowledge, no spectrum of *Typhon* has been published. The one we present in this work shows an absorption band due to water ice at 2.0 microns that is $11 \pm 3\%$ deep, but shows no clear evidence of any feature in the H band (Fig. 1a). The water ice fraction found by the best fit model is 5% (39 microns grains), but as much as 10% to 20% could be present (see Fig. 8). *Typhon* is the smallest TNO of our sample (diameter of about 175 km), but since it is a binary, each component might even be smaller. The detection of water ice on such a small – and thus geologically inert – body is an important clue in our understanding of the water ice state in the outer Solar System. This will be investigated in Alvarez-Candal et al. (in preparation).

Thereus Barucci et al. (2002) observed *Thereus* at two different epochs in 2001 and found different spectra: either featureless, or showing clear absorption bands at 1.5 and 2.0 microns, due to the presence of water ice. This leads to the conclusion that *Thereus*'s surface is clearly inhomogeneous. Those heterogeneities have been

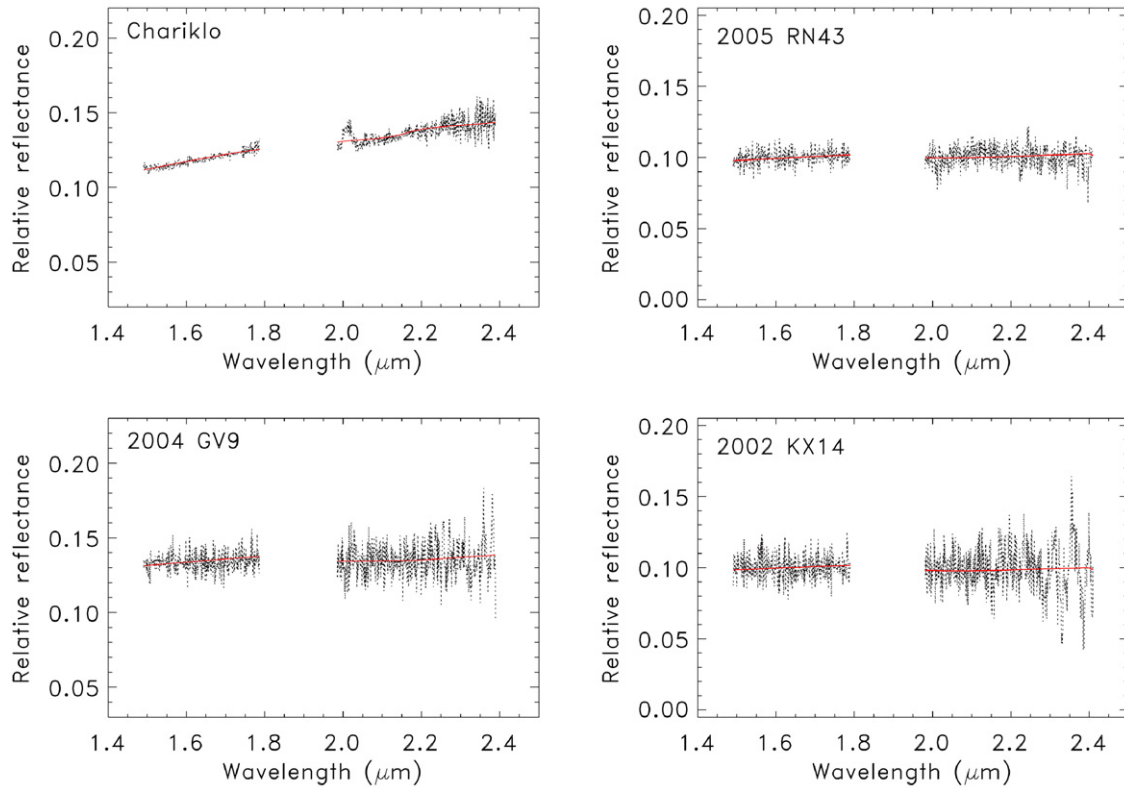


Fig. 5. *Featureless spectra.* The dotted lines represent the H + K reflectance spectra, with spectral resolution of 1500. Each spectrum has been normalized around 1.65 μm to the estimated H-albedo. The best fit model of each spectrum is overlotted in solid line. The upper left plot corresponds to Chariklo. A feature is present around 2.05 microns that we attribute to imperfect removal of telluric absorption. The best fit model includes no water ice. The upper right plot shows the spectrum of 2005 RN₄₃ as long as its best fit model, obtained with 1% of crystalline water ice. The lower left plot corresponds to 2004 GV₉: the best fit includes 1% of amorphous water ice, and the lower right plot corresponds to 2002 KX₁₄. The best fit model is obtained with 2% of crystalline water ice.

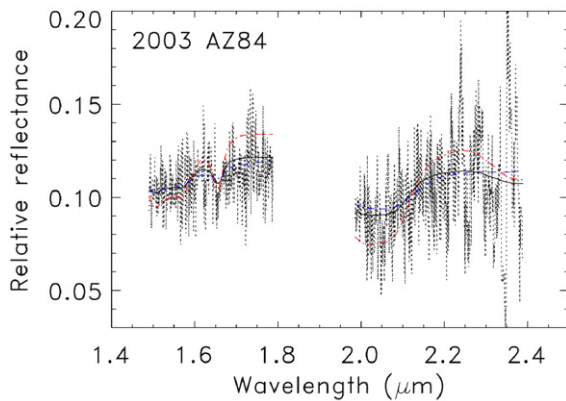


Fig. 6. *2003 AZ₈₄.* H + K reflectance spectrum of 2003 AZ₈₄ in dotted line. The best fit model is shown in solid line: it corresponds to 17% of water ice (15% crystalline, 2% amorphous, reduced $\chi^2 = 4.176 \times 10^{-3}$). The dashed line corresponds to 8.5% of water ice (7.5% crystalline, 1% amorphous, reduced $\chi^2 = 4.225 \times 10^{-3}$) and the dot-dashed line to 34% of water ice (30% crystalline, 4% amorphous, reduced $\chi^2 = 5.082 \times 10^{-3}$).

then confirmed by Licandro and Pinilla-Alonso (2005), who observed 8 spectra during more than half a rotation of the object. From their modeling, they found that the amount of water ice could vary from 0 to 25%. Merlin et al. (2005) also confirmed those inhomogeneities on the surface of Thereus. Our spectrum shows the 2.0 microns absorption band due to water ice (depth of $10 \pm 3\%$), but no evidence of any absorption feature in the H band (Fig. 1b). The best fit model is found with a crystalline water ice amount of 18% with 10 microns grains, although as much as 35% of water ice could be present within the noise (see Fig. 9).

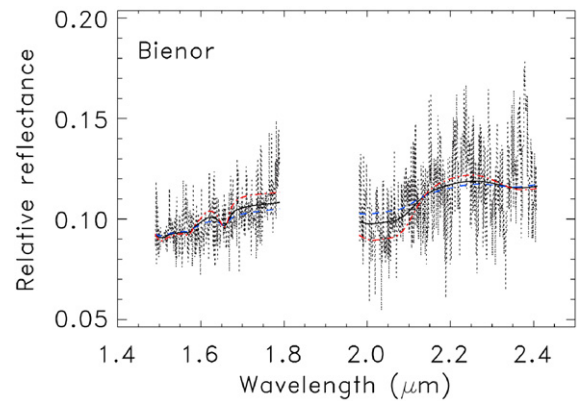


Fig. 7. *Bienor.* H + K reflectance spectrum of Bienor in dotted line. The best fit model is shown in solid line: it corresponds to 13% of crystalline water ice (reduced $\chi^2 = 2.604 \times 10^{-3}$). The dashed line corresponds to 7% of crystalline water ice (reduced $\chi^2 = 2.198 \times 10^{-3}$) and the dot-dashed line to 26% of crystalline water ice (reduced $\chi^2 = 2.656 \times 10^{-3}$).

4.3.2. Ambiguous cases

Crantor Doressoundiram et al. (2005) found no feature at 1.5 microns in Crantor spectrum, but detected one at 2.0 microns. They therefore suggested the presence of water ice. Barkume et al. (2008) confirmed the presence of water ice. Doressoundiram et al. (2005) also found a feature at 2.3 microns, maybe due to the presence of some methanol-like compound, which has been confirmed in Alvarez-Candal et al. (2007). Our spectrum is noisy, and no feature can be detected (Fig. 2a). We computed the depth of a possible absorption band at 2.0 microns and found that it could be $6 \pm 4\%$ deep. The high level of noise around 2.3 microns does not allow us to draw any reliable conclusion on the possible pres-

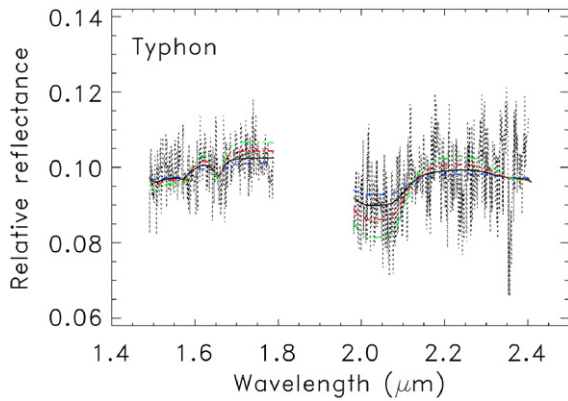


Fig. 8. *Typhon*. H + K reflectance spectrum of *Typhon* in dotted line. The best fit model is shown in solid line: it corresponds to 5% of crystalline water ice (reduced $\chi^2 = 5.233 \times 10^{-4}$). The dashed line corresponds to 3% of crystalline water ice (reduced $\chi^2 = 2.917 \times 10^{-3}$), the dot-dashed line to 10% of crystalline water ice (reduced $\chi^2 = 4.916 \times 10^{-3}$) and the three dot-dashed line to 20% of crystalline water ice (reduced $\chi^2 = 2.472 \times 10^{-2}$).

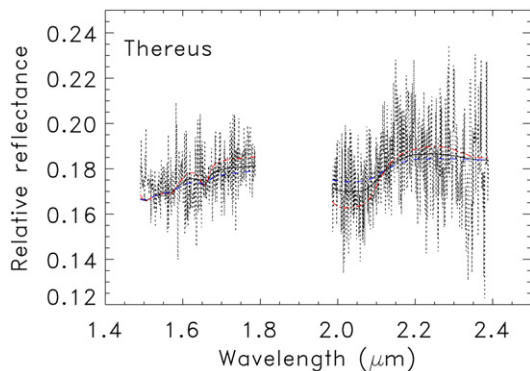


Fig. 9. *Thereus*. H + K reflectance spectrum of *Thereus* in dotted line. The best fit model is shown in solid line: It corresponds to 18% of crystalline water ice (reduced $\chi^2 = 1.025 \times 10^{-3}$). The dashed line corresponds to 9% of crystalline water ice (reduced $\chi^2 = 1.047 \times 10^{-3}$), and the dot-dashed line to 35% of crystalline water ice (reduced $\chi^2 = 1.096 \times 10^{-3}$).

ence of a feature at 2.3 microns. Our best fit model is obtained with no water ice (see Fig. 10). Since there is no clear detection of any feature in Crantor's spectrum, we cannot confirm the presence of water ice, though significant amounts of ice could be present without being detected within the noise.

Ixion Licandro et al. (2002) found that *Ixion*'s spectrum was featureless, without any feature at 1.5 and 2.0 microns. Boehnhardt et al. (2004) combined this near-infrared spectrum with their visible spectrum, and found from spectral modeling by a geographical mixture that the surface could be composed of a very small amount of water ice only (2%). Barkume et al. (2008) detected a larger amount of water ice. Our spectrum is almost featureless in the H band, but could show an absorption band at 2.0 microns, that is $7 \pm 4\%$ deep (Fig. 2a). We found a best fit model with an amount of 16% of amorphous water ice (10 microns grains, Fig. 10), while up to 30% could be present within the noise.

1999 TC₃₆ Dotto et al. (2003a) and Merlin et al. (2005) tried to model the spectrum of 1999 TC₃₆ with different chemical compositions but both found a water ice amount of 8%. On the other hand, Barkume et al. (2008) found a much larger amount of water ice. The spectrum presented here is rather flat and featureless, though a small absorption band can be detected at 2.0 microns (Fig. 2a) (this feature is $4 \pm 3\%$ deep). We tried to find the maximum amount of water ice that could be present on the surface

without being detected within the noise: our best fit model corresponds to an amount of 9% of amorphous water ice (10 microns grains, Fig. 10). We can therefore conclude that 1999 TC₃₆ might present rotational inhomogeneities that could explain the different amounts of water ice found in spectra taken at different moments. NACO data taken in the framework of this Large Program confirm this possibility: all those results will be presented along with visible, J spectra and modeling in Protospapa et al. (2009).

Echeclus We present in this work a new near-infrared spectrum of *Echeclus* (Fig. 2a). Although *Echeclus*' spectrum should be classified as featureless from our analysis, we decided to consider it as an ambiguous case since its spectral behavior is not featureless. The shape of the H band shows a decrease of the reflectivity beyond 1.7 microns, that we attribute to poorly corrected atmospheric absorption. A single solar analog was available for this night, which did not allow us to perform a proper correction of this feature. The overall spectrum is featureless, though a decrease of the reflectivity around 2.0 microns could be considered as a feature due to water ice. The calculation of the depth of this possible band leads to a negative value, which is inconsistent with any absorption band. This may be due to the feature around 1.7 microns, that makes the algorithm fail when trying to compute the depth of a possible 2.0 microns absorption band, since it cannot estimate the continuum properly. Nonetheless, the best fit for this spectrum is found with no water ice (Fig. 10). Therefore, we cannot draw any firm conclusion regarding the presence of water ice on *Echeclus*.

2002 AW₁₉₇ A first spectrum obtained by Doressoundiram et al. (2005) indicated the presence of water ice on 2002 AW₁₉₇'s surface, confirmed by Barkume et al. (2008). Our spectrum shows an absorption band centered at 2.05 microns, attributed to incomplete removal of telluric features. Indeed, one single solar analog was available for this observation night, which did not allow us to perform a proper correction of this band (Fig. 2a). Apart from this feature, the general behavior of the spectra is featureless and flat (spectral gradient of $0.11 \pm 0.34\%$ per 0.1 micron). The 2.0 microns band – if present – could be hidden by the noise, and by the feature previously discussed, as can be seen in Fig. 10. Indeed, our best fit model is found with 17% of crystalline water ice (10 microns grains). Considering the lack of absorption band detection, we cannot draw a reliable conclusion on the presence of water ice on 2002 AW₁₉₇'s surface.

1999 DE₉ Jewitt and Luu (2001) found evidences of features at 2.0 microns and around 1.5 microns in 1999 DE₉ spectrum. They therefore suggested the presence of water ice on its surface. Nonetheless, those features were not confirmed neither by Alvarez-Candal et al. (2007), nor by Barkume et al. (2008), who found a featureless spectrum within the noise. The spectrum observed in the framework of this Large Program present the featureless behavior, confirming the results recently found (Fig. 2b). However, the best fit model has been found with 4% of water ice, with 10 microns grains (Fig. 10).

2000 GN₁₇₁ This object might be subject to rotational inhomogeneities as suggested by de Bergh et al. (2004). They found a red spectral gradient between the H and K bands, and no ice had been detected on its spectrum. Alvarez-Candal et al. (2007) and Barkume et al. (2008) found similar spectra, featureless and flat, different from the de Bergh et al. (2004) spectrum, which is in good agreement with the hypothesis of rotational inhomogeneities. Our new spectrum confirms the behavior found by Alvarez-Candal et al. (2007): 2000 GN₁₇₁ spectrum is rather blue (spectral gradient of $-1.46 \pm 0.34\%$ per 0.1 micron) and featureless (Fig. 2b). However, 9% of water ice is found by the best fit model (22 microns

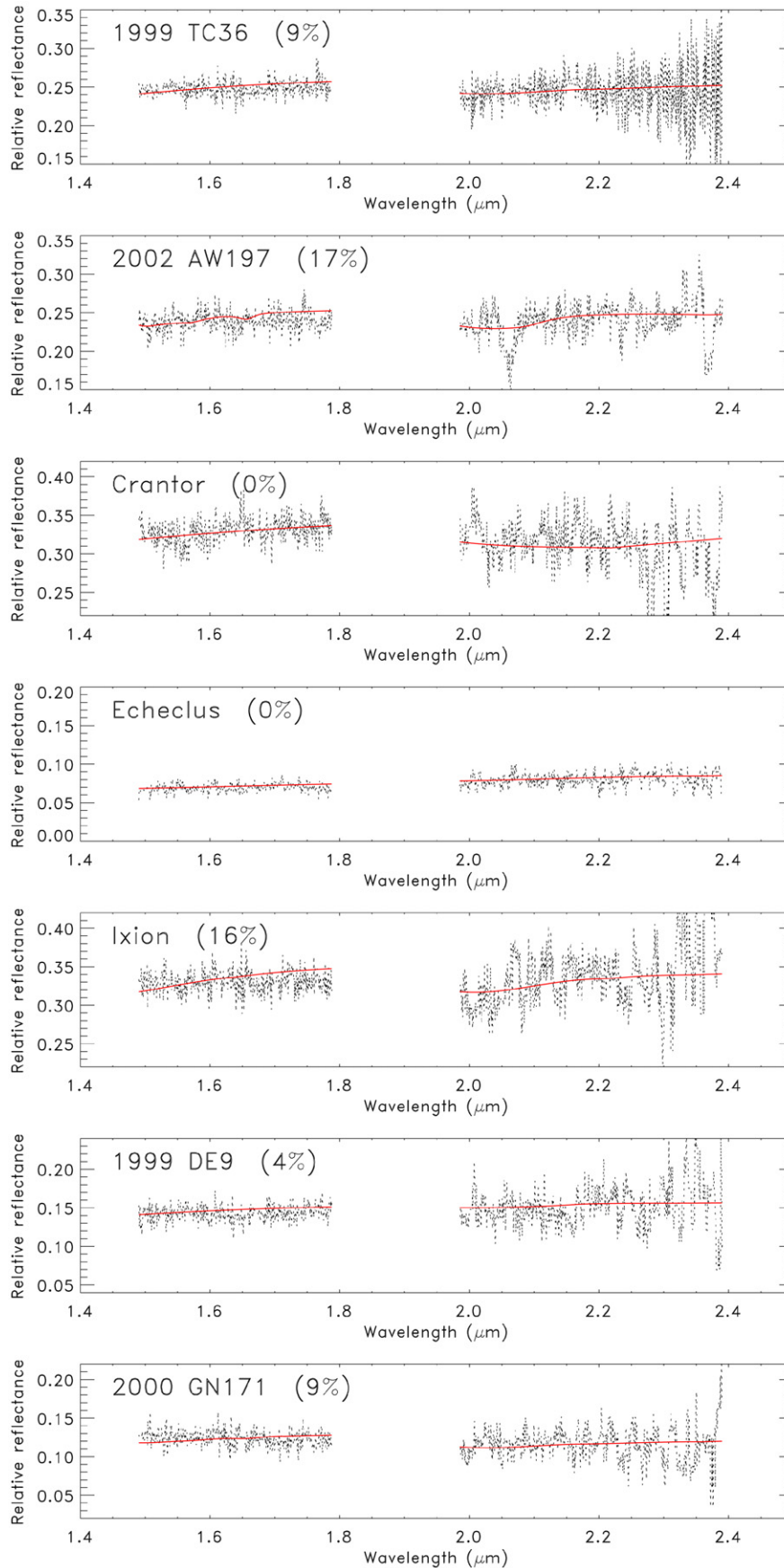


Fig. 10. *Ambiguous cases.* The spectra of these 7 objects are presented in dotted lines. Each spectrum has been normalized around 1.65 μm to the estimated H-albedo. The best fit model of each spectrum is overplotted in solid line. Downwards, we get the spectrum of 1999 TC₃₆, 2002 AW₁₉₇, Crantor, Echeclus, Ixion, 1999 DE₉ and 2000 GN₁₇₁. The best fit models include respectively 9%, 17%, 0%, 0%, 16%, 4% and 9% of water ice (see details in Table 3).

grains, Fig. 10). The analysis suggests that a significant amount of water ice should be present on 2000 GN₁₇₁'s surface.

4.4. Noisiest cases

1996 TL₆₆ 1996 TL₆₆ had been first observed by Luu and Jewitt (1998) who found that no ice was present on its surface. We re-observed this object, but due to unstable weather conditions, the resulting signal to noise ratio is poor (Fig. 2b), and when trying to model this spectrum, the best fit is given with an amount of 28% of water ice (23 microns grains).

2003 FY₁₂₈ Barkume et al. (2008) found an amount of 18% of crystalline water ice on the surface of 2003 FY₁₂₈. Our spectrum is very noisy, and no absorption band can be detected (Fig. 2b). We run the modeling described in Section 3 to fit this spectrum, and found 1% water ice to be present on 2003 FY₁₂₈'s surface (10 microns grains, red mixture). However, 10 or 20% of water ice could be present on the surface, without being detected within the noise.

2003 QW₉₀ The 2003 QW₉₀'s spectrum presented in this work is the bluest that we observed during this first year of ESO Large Program: the spectral gradient computed for the H + K region is $-3.41 \pm 0.49\%$ per micron (Fig. 2b). Because of the noise, this value is not really reliable. From spectral modeling, no water ice has been found but as much as 20% could be present within the noise.

5. Conclusion

In this paper, we presented the near-infrared H+K spectra of 21 objects, including 4 objects never observed before, to our knowledge. The observations were performed with SINFONI, mounted on VLT-UT4, in the framework of the first year of an ESO-Large Program. We obtained high quality data for most of the objects, enabling a search for the presence of possible absorption bands. Though our data quality is very good, some new spectra with even higher quality would be needed to draw conclusions on the detections of some absorption bands. Indeed, even with a 8.2-m telescope, observing such faint objects means reaching the limits of both the telescope and the instrument.

Methane ice is detected on Eris's surface, without any shift in the central wavelengths of the absorption bands. We searched for the possible presence of water ice in the 20 other spectra, and detected H₂O on six objects: Orcus, Quaoar, 2003 AZ₈₄, Bienor, Thereus and Typhon. The spectra of Orcus and Quaoar show features at 1.5, 1.65 and 2.0 microns due to crystalline water ice, and a small feature around 2.2 microns that can be attributed either to ammonia hydrates or to methane ice. The best fit model of Orcus's spectrum presented in Barucci et al. (2008a) included a small amount of ammonia hydrate. Recent resurfacing processes due to internal activity are therefore suggested, since the surface should be depleted of this volatile in less than 10⁷ years (Cooper et al., 2003). In the case of Quaoar, the high signal to noise ratio allows the unambiguous detection of a small feature at 1.724 microns due to the presence of methane ice. The 2.2 microns absorption band is consequently attributed to methane, as suggested by Schaller and Brown (2007). Since CH₄ is more stable to irradiation than ammonia, no recent resurfacing process is implied: Quaoar might be geologically dead and in the process of losing its volatiles. Its surface does not show any heterogeneity. A 3D thermal model under development in our group is being applied to these bodies to constrain the possibility of internal geologic processes.

For 7 objects, no absorption bands are visible, but the level of noise can hide possible features. Water ice could be present on the surface of Crantor, Ixion, 1999 TC₃₆, Echeclus, 1999 DE₉,

2000 GN₁₇₁ and 2002 AW₁₉₇. We thus need higher quality data to draw reliable conclusions on these objects.

Three spectra are too noisy to draw any conclusion, although water ice could be present on their surfaces: 1996 TL₆₆, 2003 QW₉₀ and 2003 FY₁₂₈.

Four spectra — Chariklo, 2004 GV₉, 2002 KX₁₄, 2005 RN₄₃ — are featureless. Since irradiation causes the progressive formation of a crust obscuring the possible ices underneath, the non-detection does not mean that water ice is not present within, even near the surface of, these objects. Due to the high quality of the data, we can conclude that no water ice is present on the layers probed by the 1.49–2.4 microns wavelength range. The case of Chariklo is even more interesting since water ice had been unambiguously detected in previous works, which implies a strongly heterogeneous surface.

Finally, we estimated that if we take into account uncertainties due to the spectra noise level, most objects may contain up to an additional 10% of water ice amount. We want to stress that direct comparisons of water ice contents with other works have to be made with care, since they strongly depend on the grains size, the type of mixture and its components, and the model that is used, as well as the wavelength range on which it is applied. Comparisons of the 2.0 microns band depth are more reliable. We find that the surface of Quaoar, 2002 KX₁₄ and 2005 RN₄₃ should be homogeneous, while on the contrary, Chariklo, 2000 GN₁₇₁ and maybe 2003 AZ₈₄ should present rotational inhomogeneities that will be investigated.

Acknowledgments

We thank R. Davies for the great help he provided with the sky estimation and correction, and A. Modigliani, who highlighted the subtleties of the ESO-SINFONI pipeline. We also want to thank J. Emery and an anonymous referee for their useful comments.

References

- Alvarez-Candal, A., Barucci, M.A., Merlin, F., Guilbert, A., de Bergh, C., 2007. A search for rotational variations on trans-neptunian objects. *Astron. Astrophys.* 475, 369–374.
- Alvarez-Candal, A., Fornasier, S., Barucci, M.A., de Bergh, C., Merlin, F., 2008. Visible spectroscopy of the new ESO Large Program on trans-neptunian objects and Centaurs. Part 1. *Astron. Astrophys.* 487, 741–748.
- Barkume, K.M., Brown, M.E., Schaller, E.L., 2008. Near-infrared spectra of Centaurs and Kuiper belt objects. *Astron. J. Lett.* 135, 55–67.
- Barucci, M.A., and 19 colleagues, 2002. Visible and near-infrared spectroscopy of the Centaur 32532 (2001 PT13). ESO Large Program on TNOs and Centaurs: First spectroscopy results. *Astron. Astrophys.* 392, 335–339.
- Barucci, M.A., Merlin, F., Guilbert, A., de Bergh, C., Alvarez-Candal, A., Hainaut, O., Doressoundiram, A., Dumas, C., Owen, T., Coradini, A., 2008a. Surface composition and temperature of the TNO Orcus. *Astron. Astrophys.* 479, 13–16.
- Barucci, M.A., Brown, M.E., Emery, J.P., Merlin, F., 2008b. Composition and surface properties of transneptunian objects and Centaurs. In: Barucci, M.A., Boehnhardt, H., Cruikshank, D., Morbidelli, A. (Eds.), *The Solar System beyond Neptune*. University of Arizona Press, Tucson, pp. 143–160.
- Belskaya, I., Bagnulo, S., Muinonen, K., Barucci, M.A., Tozzi, G.P., Fornasier, S., Kolokolova, L., 2008. Polarimetry of the dwarf planet (136199) Eris. *Astron. Astrophys.* 479, 265–269.
- Boehnhardt, H., Bagnulo, S., Muinonen, K., Barucci, M.A., Kolokolova, L., Dotto, E., Tozzi, G.P., 2004. Surface characterization of 28978 Ixion (2001 KX76). *Astron. Astrophys.* 415, 21–25.
- Brown, M.E., Koresko, C.C., 1998. Detection of water ice on the Centaur 1997 CU 26. *Astron. Astrophys. J.* 505, 65–67.
- Brown, M.E., Trujillo, C.A., Rabinowitz, D.L., 2005. Discovery of a planetary-sized object in the scattered Kuiper belt. *Astron. Astrophys. J.* 635, 97–100.
- Brown, R.H., Cruikshank, D.P., Pendleton, Y., Veeder, G.J., 1998. Identification of water ice on the Centaur 1997 CU26. *Science* 280, 1430–1432.
- Brunetto, R., Roush, T.L., 2008. Impact of irradiated methane ice crusts on compositional interpretations of TNOs. *Astron. Astrophys.* 481, 879–882.
- Cook, J.C., Desch, S.J., Roush, T.L., Trujillo, C.A., Geballe, T.R., 2007. Near-infrared spectroscopy of Charon: Possible evidence for cryovolcanism on Kuiper belt objects. *Astron. Astrophys. J.* 663, 1406–1419.

- Cooper, J.F., Christian, E.R., Richardson, J.D., Wang, C., 2003. Proton irradiation of Centaurs, Kuiper belt, and Oort Cloud objects at plasma to cosmic ray energy. *Earth Moon Planets* 92, 261–277.
- Davies, R.I., 2007. A method to remove residual OH emission from near-infrared spectra. *Mon. Not. R. Astron. Soc.* 375, 1099–1105.
- de Bergh, C., Boehnhardt, H., Barucci, M.A., Lazzarin, M., Fornasier, S., Romon-Martin, J., Tozzi, G.P., Doressoundiram, A., Dotto, E., 2004. Aqueous altered silicates at the surface of two Plutinos? *Astron. Astrophys.* 416, 791–798.
- de Bergh, C., Delsanti, A., Tozzi, G.P., Dotto, E., Doressoundiram, A., Barucci, M.A., 2005. The surface of the transneptunian object 90482 Orcus. *Astron. Astrophys.* 437, 1115–1120.
- DeMeo, F.E., Fornasier, S., Barucci, M.A., Perna, D., Protopapa, S., Alvarez-Candal, A., Delsanti, A., Doressoundiram, A., Merlin, F., de Bergh, C., 2009. Visible and near-infrared colors of TNOs and Centaurs from the second ESO Large Program. *Astron. Astrophys.* 493, 283–290.
- De Sanctis, M.C., Capria, M.T., Coradini, A., 2001. Thermal evolution and differentiation of Edgeworth–Kuiper belt objects. *Astron. J.* 121, 2792–2799.
- Doressoundiram, A., Barucci, M.A., Tozzi, G.P., Poulet, F., Boehnhardt, H., de Bergh, C., Peixinho, N., 2005. Spectral characteristics and modeling of the trans-neptunian object (55565) 2002 AW197 and the Centaurs (55576) 2002 GB10 and (83982) 2002 G09: ESO Large Program on TNOs and Centaurs. *Planet. Space Sci.* 53, 1501–1509.
- Doressoundiram, A., Boehnhardt, H., Tegler, S.C., Trujillo, C., 2008. Color properties and trends of the transneptunian objects. In: Barucci, M.A., Boehnhardt, H., Cruikshank, D., Morbidelli, A. (Eds.), *The Solar System beyond Neptune*. University of Arizona Press, Tucson, pp. 91–104.
- Dotto, E., Barucci, M.A., Boehnhardt, H., Romon, J., Doressoundiram, A., Peixinho, N., de Bergh, C., Lazzarin, M., 2003a. Searching for water ice on 47171 1999 TC36, 1998 SG35, and 2000 QC243: ESO Large Program on TNOs and Centaurs. *Icarus* 162, 408–414.
- Dotto, E., Barucci, M.A., Leyrat, C., Romon, J., de Bergh, C., Licandro, J., 2003b. Unveiling the nature of 10199 Chariklo: Near-infrared observations and modeling. *Icarus* 164, 122–126.
- Dotto, E., Perna, D., Barucci, M.A., Rossi, A., de Bergh, C., Doressoundiram, A., Fornasier, S., 2008. Rotational properties of Centaurs and trans-neptunian objects lightcurves and densities. *Astron. Astrophys.* 490, 829–833.
- Dumas, C., Merlin, F., Barucci, M.A., de Bergh, C., Hainaut, O., Guilbert, A., Vernazza, P., Doressoundiram, A., 2007. Surface composition of the largest dwarf planet 136199 Eris (2003 UB313). *Astron. Astrophys.* 471, 331–334.
- Eisenhauer, F., and 22 colleagues, 2003. SINFONI—Integral field spectroscopy at 50 milli-arcsecond resolution with the ESO VLT. In: Iye, M., Moorwood, A.F.C. (Eds.), *Instrument Design and Performance for Optical/Infrared Ground-Based Telescopes*. In: *Proc. of the SPIE*, vol. 4841, pp. 1548–1561.
- Fornasier, S., Dotto, E., Barucci, M.A., Barbieri, C., 2004. Water ice on the surface of the large TNO 2004 DW. *Astron. Astrophys.* 422, 43–46.
- Fulchignoni, M., Belskaya, I., Barucci, M.A., de Sanctis, M.C., Doressoundiram, A., 2008. Transneptunian object taxonomy. In: Barucci, M.A., Boehnhardt, H., Cruikshank, D., Morbidelli, A. (Eds.), *The Solar System beyond Neptune*. University of Arizona Press, Tucson, pp. 181–192.
- Grundy, W.M., Schmitt, B., 1998. The temperature-dependent near-infrared absorption spectrum of hexagonal formula H₂O ice. *J. Geophys. Res.* 103, 25809–25822.
- Guilbert, A., Barucci, M.A., Brunetto, R., Delsanti, A., Merlin, F., Alvarez-Candal, A., Fornasier, S., de Bergh, C., Sarid, G., 2009. A portrait of Centaur 10199 Chariklo. *Astron. Astrophys.*, submitted for publication.
- Hainaut, O.R., Delahodde, C.E., Boehnhardt, H., Dotto, E., Barucci, M.A., Meech, K.J., Bauer, J.M., West, R.M., Doressoundiram, A., 2000. Physical properties of TNO 1996 TO66. Lightcurves and possible cometary activity. *Astron. Astrophys.* 356, 1076–1088.
- Jewitt, D., Luu, J., 1993. Discovery of the candidate Kuiper belt object 1992 QB1. *Nature* 362, 730–732.
- Jewitt, D.C., Luu, J.X., 2001. Colors and spectra of Kuiper belt objects. *Astron. J.* 122, 2099–2114.
- Jewitt, D.C., Luu, J., 2004. Crystalline water ice on the Kuiper belt object (50000) Quaoar. *Nature* 432, 731–733.
- Khare, B.N., Thompson, W.R., Cheng, L., Chyba, C., Sagan, C., Arakawa, E.T., Meisse, C., Tuminello, P.S., 1993. Production and optical constraints of ice tholin from charged particle irradiation of (1:6) C₂H₆/H₂O at 77 K. *Icarus* 103, 290–300.
- Licandro, J., Pinilla-Alonso, N., 2005. The inhomogeneous surface of Centaur 32522 Thereus (2001 PT13). *Astrophys. J.* 630, 93–96.
- Licandro, J., Ghinassi, F., Testi, L., 2002. Infrared spectroscopy of the largest known trans-neptunian object 2001 KX75. *Astron. Astrophys.* 388, 9–12.
- Licandro, J., Grundy, W.M., Pinilla-Alonso, N., Leisy, P., 2006. Visible spectroscopy of 2003 UB313: Evidence for N₂ ice on the surface of the largest TNO? *Astron. Astrophys.* 458, 5–8.
- Luu, J.X., Jewitt, D.C., 1998. Optical and infrared reflectance spectrum of Kuiper belt object 1996 TL 66. *Astrophys. J.* 494, 117–120.
- McDonald, G.D., Whited, L.J., Deruiter, C., Khare, B.N., Patnaik, A., Sagan, C., 1996. Production and chemical analysis of cometary ice tholins. *Icarus* 122, 107–117.
- McKinnon, W.B., 2002. On the initial thermal evolution of Kuiper belt objects. In: Warmbein, B. (Ed.), *Proc. Asteroids, Comets, and Meteors: ACM 2002*. In: *ESA Special Publication*, vol. 5000. Noordwijk, Netherlands, pp. 29–38.
- Meech, K.J., Belton, M.J.S., 1990. The atmosphere of 2060 Chiron. *Astron. J.* 100, 1323–1338.
- Merk, R., Prialnik, D., 2006. Combined modeling of thermal evolution and accretion of trans-neptunian objects—Occurrence of high temperatures and liquid water. *Icarus* 183, 283–295.
- Merlin, F., Barucci, M.A., Dotto, E., de Bergh, C., Lo Curto, G., 2005. Search for surface variations on TNO 47171 and Centaur 32532. *Astron. Astrophys.* 444, 977–982.
- Merlin, F., Guilbert, A., Dumas, C., Barucci, M.A., de Bergh, C., Vernazza, P., 2007. Properties of the icy surface of the TNO 136108 (2003 EL61). *Astron. Astrophys.* 466, 1185–1188.
- Merlin, F., Alvarez-Candal, A., Delsanti, A., Fornasier, S., Barucci, M.A., DeMeo, F.E., de Bergh, C., Doressoundiram, A., Quirico, E., Schmitt, B., 2009. Stratification of methane ice on Eris' surface. *Astron. J.* 137, 315–328.
- Pinilla-Alonso, N., Licandro, J., Gil-Hutton, R., Brunetto, R., 2007. The water ice rich surface of (145453) 2005 RR43: A case for a carbon-depleted population of TNOs? *Astron. Astrophys.* 468, 25–28.
- Protopapa, S., Alvarez-Candal, A., Barucci, M.A., Tozzi, G.P., Fornasier, S., Delsanti, A., Merlin, F., 2009. Surface variations on (47171) 1999 TC36: ESO large program on TNOs. *Astron. Astrophys.*, submitted for publication.
- Rousselot, P., 2008. 174P/Echeclus: A strange case of outburst. *Astron. Astrophys.* 480, 543–550.
- Schaller, E.L., Brown, M.E., 2007. Detection of methane on Kuiper belt object (50000) Quaoar. *Astrophys. J.* 670, 49–51.
- Schmitt, B., Quirico, E., Trotta, F., Grundy, W.M., 1998. Optical properties of ices from UV to infrared. In: Schmitt, B., de Bergh, C., Festou, M. (Eds.), *Solar System Ices*. In: *Astrophysics and Space Science Library*, vol. 227. Kluwer Academic, Dordrecht, pp. 199–240.
- Shkuratov, Y., Starukhina, L., Hoffmann, H., Arnold, G., 1999. A model of spectral albedo of particulate surfaces: Implications for optical properties of the Moon. *Icarus* 137, 235–246.
- Shul'man, L.M., 1972. The chemical composition of cometary nuclei. In: Chebotarev, G.A., Kazimirchak-Polonskaia, E.I., Marsden, B.G. (Eds.), *The Motion, Evolution of Orbits, and Origin of Comets*, IAU Symposium 45. Reidel, Dordrecht, pp. 265–270.
- Stansberry, J., Grundy, W., Brown, M., Cruikshank, D., Spencer, J., Trilling, D., Margot, J.-L., 2008. Physical properties of Kuiper belt and Centaur objects: Constraints from the Spitzer Space Telescope. In: Barucci, M.A., Boehnhardt, H., Cruikshank, D., Morbidelli, A. (Eds.), *The Solar System beyond Neptune*. University of Arizona Press, Tucson, pp. 161–179.
- Strazulla, G., Palumbo, M.E., 1998. Evolution of icy surfaces: An experimental approach. *Planet. Space Sci.* 46, 1339–1348.
- Thompson, W.R., Murray, B.G.J.P.T., Khare, B.N., Sagan, C., 1987. Coloration and darkening of methane clathrate and other ices by charged particle irradiation—Applications to the outer Solar System. *J. Geophys. Res.* 92, 14933–14947.
- Trujillo, C.A., Brown, M.E., Rabinowitz, D.L., Geballe, T.R., 2005. Near-infrared surface properties of the two intrinsically brightest minor planets: (90377) Sedna and (90482) Orcus. *Astrophys. J.* 627, 1057–1065.
- Trujillo, C.A., Brown, M.E., Barkume, K.M., Schaller, E.L., Rabinowitz, D.L., 2007. The surface of 2003 EL61 in the near-infrared. *Astrophys. J.* 655, 1172–1178.
- Zheng, W., Jewitt, D., Kaiser, R.I., 2008. Amorphization of crystalline water ice. *ArXiv e-prints*, 801.